

LIPSCHITZ RECURRENT NEURAL NETWORKS

N. BENJAMIN ERICHSON[♥], OMRI AZENCOT[♦], ALEJANDRO QUEIRUGA[♣] AND MICHAEL W. MAHONEY[♥]

ABSTRACT. Differential equations are a natural choice for modeling recurrent neural networks because they can be viewed as dynamical systems with a driving input. In this work, we propose a recurrent unit that describes the hidden state’s evolution with two parts: a well-understood linear component plus a Lipschitz nonlinearity. This particular functional form simplifies stability analysis, which enables us to provide an asymptotic stability guarantee. Further, we demonstrate that Lipschitz recurrent units are more robust with respect to perturbations. We evaluate our approach on a range of benchmark tasks, and we show it outperforms existing recurrent units.

1 INTRODUCTION

Many interesting problems exhibit temporal structures that can be well-modeled with recurrent neural networks (RNNs), including problems in robotics, natural language processing, system identification, and machine learning control. In contrast to feed-forward neural networks, RNNs consist of one or more recurrent units that are designed to have dynamical (recurrent) properties, thereby enabling them to acquire some form of internal memory. This equips RNNs with the ability to discover and exploit certain patterns, such as symmetries and periodic structures [1]. However, RNNs are widely-known to have stability issues and are notoriously difficult to train, most notably due to the vanishing and exploding gradients problem [2, 3].

Most state-of-the-art recurrent units deal with the vanishing and exploding gradients issue by restricting the hidden-to-hidden weight matrix, *e.g.*, to be an element of the orthogonal group [4, 5, 6, 7]. While such an approach is advantageous, it limits the expressivity of the model. To address the expressivity problem, recent work has parameterized the recurrent unit so that the hidden-to-hidden matrix has unit norm eigenvalues and is sampled from a larger set of matrices [8, 9].

In this work, we address these challenges by viewing RNNs as dynamical systems whose temporal evolution is governed by an abstract system of differential equations with an external input. The data are formulated in continuous-time where the external input is defined by the function $x = x(t) \in \mathbb{R}^p$, and the target signal is defined by $y = y(t) \in \mathbb{R}^d$. Based on insights from dynamical systems theory, we propose a continuous-time Lipschitz recurrent neural network with the functional form

$$\begin{aligned} (1a) \quad & \dot{h} = Ah + \tanh(Wh + Ux + b), \\ (1b) \quad & y = Dh. \end{aligned}$$

Here, $h = h(t) \in \mathbb{R}^N$ is a function of time t that represents an internal (hidden) state, and $\dot{h} = \frac{\partial h(t)}{\partial t}$ is its time derivative. The hidden state represents the memory that the system has of its past. The function in Eq. (1a) is parameterized by the hidden-to-hidden weight matrices $A \in \mathbb{R}^{N \times N}$ and $W \in \mathbb{R}^{N \times N}$, the input-to-hidden encoder matrix $U \in \mathbb{R}^{N \times p}$, and an offset b . The function in Eq. (1b) is parameterized by the hidden-to-output decoder matrix $D \in \mathbb{R}^{d \times N}$. Nonlinearity is

[♥] ICSI and Department of Statistics at University of California, Berkeley.

[♦] Department of Mathematics at University of California, Los Angeles.

[♣] Google, LLC.

Corresponding author: N. Benjamin Erichson (erichson@berkeley.edu).

introduced via the 1-Lipschitz tanh activation function. Systems such as this which describe the evolution of a state h as a linear component plus a Lipschitz nonlinearity, are known as *Lipschitz nonlinear systems* [10, 11, 12]. While RNNs that are governed by differential equations with an additive structure have been studied before [13, 14, 15, 16, 17, 18], the specific formulation which we propose in Eq. (1a) is distinct, and we will illustrate that it has several advantages.

The motivation for viewing RNNs as dynamical systems is that it allows us to borrow tools from stability analysis to study the long-term behavior of the hidden state. From this point of view, an unstable unit presents an exploding gradients problem, whereas the gradients of a stable model do not explode over time [19]. On the other hand, a stable recurrent unit can suffer from vanishing gradients, which in turn leads to catastrophic forgetting [20]. Thus, we opt for a stable model whose dynamics do not (or only very slowly do) decay over time. Importantly, stability is also a statement about the robustness of neural units with respect to small input perturbations. That is, stable models are less sensitive to small perturbations, in comparison to unstable models. Recently, Chang *et al.* [21] explored the stability properties of linearized RNNs and provided a *local* stability guarantee based on the Jacobian. In contrast, the particular structure of our recurrent model (1a) allows us to derive an *asymptotic* stability guarantee based on *Lyapunov’s direct method*. In addition, our analysis results promote the design of a symmetric-skew decomposition for hidden-to-hidden matrices which alleviates exploding and vanishing gradients, while being highly expressive and robust to input perturbations.

In summary, the main contributions of this work are:

- We use *Lyapunov’s direct method* to study the behavior of the proposed Lipschitz nonlinear system in Equation (1a). As a result, we can conclude that *the unit is stable if the matrix A has eigenvalues with negative real parts*, and it is unstable otherwise (Sec. 3).
- We propose a novel scheme, *based on the symmetric-skew decomposition*, for constructing hidden-to-hidden matrices. This scheme *mitigates the vanishing and exploding gradients* (Sec. 4), while obtaining *highly expressive* hidden-to-hidden matrices.
- We show that our Lipschitz RNN has the *ability to outperform state-of-the-art recurrent units* on tasks such as ordered and permuted pixel-by-pixel MNIST classification (Sec. 6.1) and noise padded CIFAR10 classification (Sec. 6.2).
- We demonstrate that our Lipschitz RNN is *more robust with respect to input perturbations*, compared to other continuous-time RNNs; and we study our Lipschitz RNN via the lens of the Hessian and show that it is *robust with respect to parameter perturbations* (Sec. 6.4).

2 RELATED WORK

RNNs are essentially input-output mappers, $F : \mathbb{R}^p \rightarrow \mathbb{R}^d$, that use internal feedback for learning, whereby the internal feedback is modeled via recurrent connections between basic units. The idea of learning with feedback is central to computational intelligence and can be traced back to work by McCulloch and Pitts [22] in the early 40s. Inspired by this work, in the 60s, Caianiello [23] and Rosenblatt [24] generalized the idea of learning with feedback into a framework for learning with long-term memory. The modern foundation for learning with recurrent connections was laid by Rumelhart *et al.* [25]; and work by Jordan [26] and Elman [27] helped to popularize RNNs. A simple recurrent network takes the form

$$(2) \quad h_t = \sigma(Wh_{t-1} + Ux_t),$$

$$(3) \quad y_t = Dh_t$$

where nonlinearity can be introduced via the pointwise activation function σ , such as the sigmoid or the hyperbolic tangent functions. Here, we describe just the two most relevant lines of recent work.

Unitary and orthogonal RNNs. Unitary recurrent units have received attention recently, largely due to Arjovsky *et al.* [4] who showed that unitary hidden-to-hidden matrices mitigate the vanishing and exploding gradients problem. Several other unitary and orthogonal models have also been proposed [5, 6, 28, 7, 29]. While these approaches stabilize the training process of RNNs considerably, they also limit their expressivity and their prediction accuracy. Further, unitary RNNs are expensive to train, as they typically involve the computation of a matrix inverse at each step of training. Recent work by Lezcano-Casado and Martinez-Rubio [9, 30] overcome some of these limitations. By leveraging concepts from Riemannian geometry and Lie group theory, their recurrent unit exhibits improved expressivity and predictive accuracy on a range of benchmark tasks while also being efficient to train. Another competitive recurrent design has been recently proposed by Kerg *et al.* [8]. Their approach is based on the Schur decomposition, and it enables the construction of general nonnormal hidden-to-hidden matrices with unit-norm eigenvalues.

Dynamical systems inspired RNNs. The continuous time view of RNNs has a long history in the neurodynamics community, as it provides higher flexibility and increased interpretability [31, 32]. Recently, several works have used the dynamical systems perspective to improve the stability of RNNs by introducing an antisymmetric hidden-to-hidden weight matrix; see *e.g.*, [5, 21], among others. Rubanova *et al.* [33] and De Brouwer *et al.* [34] formulate novel recurrent models for the challenging problem of irregularly-sampled and multidimensional time series data based on the theory of differential equations and their discrete integration. Similarly, Niu *et al.* [35] employ numerical methods for differential equations to study the stability of recurrent units. The link between dynamical systems and models for forecasting sequential data also provides the opportunity to incorporate physical knowledge into the learning process which improves the generalization performance, robustness, and ability to learn with limited data [36, 37, 38, 39, 40, 41, 42, 43].

3 LYAPUNOV STABILITY OF LIPSCHITZ RECURRENT UNITS

In what follows, we derive one of our key results which establishes the link between the stability of Lipschitz RNNs and the spectrum of their linear components. To this end, we briefly recall basic results from dynamical systems theory, and we refer the reader to [44] for a more detailed discussion.

Given the dynamical system, $\dot{h} = f(h)$, the study of its stability features is closely related to the equilibrium points of the system. Essentially, an equilibrium point h^* is a steady-state point for which the system is left unchanged due to repeated applications of f , *i.e.*, $f(h^*) = h^*$. To study the behavior of solutions nearby an equilibrium point, we can employ tools from dynamical systems literature. Specifically, when initialized in a small region enclosing h^* , we can determine whether the resulting trajectories of the system remain nearby, get closer (converge), or get further away (diverge). In this context, we say that an equilibrium point is stable if the associated trajectories remain close or converge to h^* . The latter notion can be formalized in the following definition.

Definition 1 (Stability in the sense of Lyapunov). *An equilibrium point h^* of $\dot{h} = f(h)$ is*

- *stable if for every $r > 0$, there exists a $\delta > 0$ such that, if $\|h(0) - h^*\| < \delta$ then*

$$(4) \quad \|h(t) - h^*\| < r, \quad \forall t > 0.$$

- *asymptotically stable if the system is stable and the equilibrium point h^* is attracting, *i.e.*, there exists a $\delta > 0$ such that, if $\|h(0) - h^*\| < \delta$ then*

$$(5) \quad \lim_{t \rightarrow \infty} h(t) - h^* = 0.$$

A useful tool for the stability analysis of dynamical systems is the direct method of Lyapunov [44, 45, 46]. Basically, Lyapunov suggests that the equilibrium point h^* is stable if there exists a *Lyapunov*

function $\mathcal{V} : \mathbb{R}^N \rightarrow \mathbb{R}$ which decreases along all trajectories close to h^* . Formally, \mathcal{V} is continuously differentiable, locally positive definite, and its time derivative is locally negative definite, *i.e.*,

$$(6) \quad \mathcal{V}(h) > 0, \quad \dot{\mathcal{V}}(h) = \langle \mathcal{V}(h), f(h) \rangle < 0, \quad \forall h \in D \setminus h^*,$$

where D is a small neighborhood around h^* , and $\mathcal{V}(h^*) = \dot{\mathcal{V}}(h^*) = 0$. We note that one of the advantages of Lyapunov’s direct method is that the stability of h^* can be determined without evaluating the vector field $f(h)$ for every $h \in \mathbb{R}^N$, which greatly simplifies its analysis and application. However, to use this method, we need to find an appropriate Lyapunov function, which is often a challenging task. Nevertheless, the specific structure of our model allows us to use a simple candidate form given by $\mathcal{V}(h) = h^\top P h$, where $P \in \mathbb{R}^{N \times N}$ is a symmetric positive definite matrix. Under this choice, we have the following result, which we prove in the supplementary material.

Proposition 1. *An equilibrium point h^* of the differential equation*

$$(7) \quad \dot{h} = Ah + \tanh(Wh + Ux + b),$$

is asymptotically stable if the eigenvalues of the hidden-to-hidden matrix A have negative real parts.

Proposition 1 requires that the nonlinearity in Eq. (1a) is Lipschitz continuous, namely, that there exists a constant $l > 0$ such that

$$(8) \quad \|g(h_1, x) - g(h_2, x)\| \leq l \|h_1 - h_2\|, \quad \forall h_1, h_2 \in \mathbb{R}^N.$$

In this work, we focus on the activation \tanh which is globally Lipschitz since its derivative is bounded by 1, and thus its Lipschitz constant is $l = 1$.

4 HIDDEN-TO-HIDDEN MATRICES VIA THE SYMMETRIC-SKEW DECOMPOSITION

In the previous section, our analysis focused on the exploding gradients problem. The following section extends the above discussion to account for the issue of vanishing gradients in the context of Lipschitz recurrent models. Specifically, based on the successful application of skew-symmetric hidden-to-hidden weights in several recent recurrent architectures, we propose an effective *symmetric-skew decomposition* for hidden matrices. Our decomposition allows for a simple control of the matrix spectrum while retaining its wide expressive range.

Recently, several methods parameterized the recurrent weights $A \in \mathbb{R}^{N \times N}$ using a skew-symmetric matrix, *i.e.*, $A + A^\top = 0$; see, *e.g.*, [5, 21]. From a stability analysis viewpoint, there are two main advantages for using skew-symmetric weights: these matrices generate the orthogonal group whose elements are isometric maps and thus preserve norms [9]; and the spectrum of skew-symmetric matrices is purely imaginary which simplifies stability analysis [21]. The main disadvantage of such a parametrization is its reduced expressivity, as these matrices have fewer than half of the parameters of a full matrix [8]. The latter limiting aspect can be explained from a dynamical systems perspective—skew-symmetric matrices can only describe oscillatory behavior, whereas a matrix whose eigenvalues have nonzero real parts can also encode viable growth and decay information.

To address the expressivity issue, we aim for hidden-to-hidden matrices which on the one hand, allow to control the expansion and shrinkage of their associated trajectories, and on the other hand, will be sampled from a larger set of matrices than those which are skew-symmetric. Our analysis in Prop. 1 guarantees that Lipschitz recurrent units maintain non-expanding trajectories if the eigenvalues of A have negative real parts. Unfortunately, this proposition does not provide any information with respect to the shrinkage of paths. Here, we opt for a system for which the amount of expansion and shrinkage can be easily controlled. Formally, the latter requirement is equivalent to designing hidden-to-hidden weights A such that $\mathcal{R}\lambda_i(A) \approx 0$, $i = 1, 2, \dots, N$. Matrices whose spectrum satisfy this constraint exhibit dynamics with moderate decay and growth behavior which alleviates the

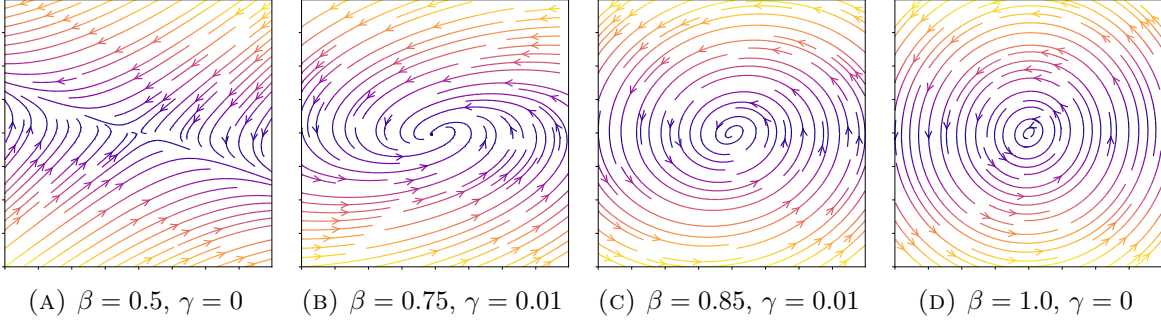


FIGURE 1. Vector fields of hidden states that are governed by Eq. (1a) trained for simple pendulum dynamics. In (a), an unstable model is shown (*i.e.*, some eigenvalues of A have positive real parts). In (b) and (c), it can be seen that the skew-symmetric decomposition leads to models that are asymptotically stable (*i.e.*, all eigenvalues of A have negative real parts), where all trajectories are attracted by an equilibrium point. In contrast, in (d), a skew-symmetric matrix ($\beta = 1$) leads to a stable model that does not have an attracting equilibrium (*i.e.*, A has purely imaginary eigenvalues).

problem of exploding and vanishing gradients. Therefore, we propose the following symmetric-skew decomposition for constructing hidden-to-hidden matrices,

$$(9) \quad A_{\beta,\gamma} = (1 - \beta) \cdot (M + M^T) + \beta \cdot (M - M^T) - \gamma I,$$

where $\beta \in [0.5, 1]$ is a tuning parameter that controls the magnitude of the eigenvalues' real parts, and $\gamma \geq 0$ shifts the real parts to the left, thus enforcing eigenvalues with non-positive real parts.

The construction $A_{\beta,\gamma}$ is useful as we can easily bound its spectrum via the tuning parameters β and γ , as we show in the next proposition. In particular, one of its consequences is that the real parts of the eigenvalues of $A_{\beta,\gamma}$ converge to zero as β tends towards one. Moreover, in the case $\beta = 1$, we recover a skew-symmetric matrix, *i.e.*, $A_{1,\gamma} + A_{1,\gamma}^T = 0$ for all γ .

Proposition 2. *Let $A_{\beta,\gamma} \in \mathbb{R}^{N \times N}$ be constructed via Eq. (9), and denote $M_{sym} := M + M^T$. Then, the real parts of the eigenvalues $\mathcal{R}\lambda_i(A_{\beta,\gamma})$, $i = 1, 2, \dots, N$, are bounded by*

$$(10) \quad (1 - \beta) \mathcal{R}\lambda_{min}(M_{sym}) - \gamma \leq \mathcal{R}\lambda_i(A_{\beta,\gamma}) - \gamma \leq (1 - \beta) \mathcal{R}\lambda_{max}(M_{sym}) - \gamma.$$

Figure 1 illustrates how different values for β and γ affect the stability behavior of the Lipschitz recurrent unit. In our experiments, values of β in the range $[0.65, 0.85]$ tend to yield the best results.

5 TRAINING CONTINUOUS-TIME LIPSCHITZ RECURRENT UNITS

Ordinary differential equations (ODEs) such as Eq. (1a) can be approximately solved by employing a certain numerical integrator. There are many techniques for numerically computing approximate solutions of differential equations, including approaches which are designed for neural network frameworks [47, 33, 48]. In what follows, we use a subscript t to denote discrete time indices, Δt represents the time difference between a pair of consecutive data points, and we define $z_t = Wh_t + Ux_{t+1} + b$. The exact and approximate solutions for h_{t+1} given h_t are given by,

$$(11) \quad h_{t+1} = h_t + \int_t^{t+\Delta t} Ah(t) + \tanh(Wh(t) + Ux(t) + b) dt$$

$$(12) \quad \approx \text{ODESolve}[Ah_t + \tanh(z_t), h_t, \Delta t],$$

$$(13) \quad = h_t + \Delta t \cdot \text{scheme}[Ah_t + \tanh(z_t), h_t, \Delta t],$$

where ODEsolve represents some choice of an integrating scheme whose application yields an approximate solution for h_{t+1} given h_t .

In this work, we consider the Implicit-Explicit (IMEX) scheme [49, 50], which is particularly well-suited to our choice of function structure in Equation (1a). Specifically, the first-order IMEX scheme in our setting takes the form

$$(14) \quad h_{t+1} = h_t + \Delta t \cdot \tanh(z_t) + \Delta t \cdot [(1 - \rho)Ah_t + \rho Ah_{t+1}],$$

where ρ is restricted to $0 \leq \rho \leq 1$, and where ϵ controls the step size. This scheme takes advantage of the fact that our Lipschitz unit is composed of a linear and a non-linear component. For $\rho = 1$, the nonlinear term would be treated explicitly (reflecting a forward Euler scheme) and the linear term is treated implicitly (reflecting a backwards Euler scheme). On the other hand, for $\rho = 0$ we obtain the explicit Euler scheme

$$(15) \quad h_{t+1} = h_t + \Delta t \cdot Ah_t + \Delta t \cdot \tanh(z_t), \quad \text{where } z_t = Wh_t + Ux_{t+1} + b.$$

In our experiments, we focus on this scheme (15) whose application yields the weights A, W, U and b after the training phase finishes. In Sec. 4, we derived a guarantee for *asymptotic stability*. We also need to consider the stability of forward Euler discretization within a time step [51]. This informs our choice of β and γ to also remain within the stability regime of forward Euler.

6 EMPIRICAL EVALUATION

In this section, we evaluate the performance of the Lipschitz RNN and compare it to other state-of-the-art methods. The model is applied to (1) ordered and (2) permuted pixel-by-pixel MNIST classification, as well as (3) pixel-by-pixel CIFAR10 and (4) a noise-padded version of CIFAR10. The latter CIFAR10 task is a particularly important test in that it requires that the recurrent unit learns long-term dependencies; that is, the hidden-to-hidden matrices need to have sufficient memory to remember information from data points that have been seen far in the past.

6.1 Ordered and Permuted Pixel-by-Pixel MNIST

The permuted pixel-by-pixel MNIST task was originally proposed as a problem to test long range dependency [52]. The 784 pixels are presented sequentially to the recurrent unit, *i.e.*, the RNN processes one pixel at a time. At the end of the sequence, the learned hidden states are used to predict the category of the MNIST image. This task requires that the recurrent unit has a sufficient long-term memory in order to discriminate between different digits. A variation to this task is to consider a fixed random permutation of the pixels, which typically poses a more challenging problem.

Table 1 provides a summary of our results. We achieve 99.0% accuracy after training the model for about 31 epochs for the ordered task. In contrast, we require about 82 epochs to reach 97.2% accuracy for the permuted task. While the model with the smaller recurrent unit ($N = 64$) performs similar on the first task, it can be seen that a larger unit, that has more capacity, is required for the permuted task. Overall, the Lipschitz recurrent unit outperforms all state-of-the-art RNNs on both tasks, while using hidden-to-hidden units of size $N = 128$. The exponential RNN [9] is the next most competitive model, yet this model requires a larger hidden-to-hidden unit to perform well.

6.2 Ordered Pixel-by-Pixel and Noise-Padded CIFAR10

A similar, yet more challenging, task is the pixel-by-pixel CIFAR10 benchmark problem that has been proposed by [21]. Again, we flatten the CIFAR10 images to construct a sequence of length 1024 in scanline order, where each element of the sequence consists of three pixels (one from each channel).

TABLE 1. Evaluation accuracy on ordered and permuted pixel-by-pixel MNIST.

Name	ordered	permuted	N	# parms
LSTM baseline by [4]	97.3%	92.7%	128	68K
Unitary RNN [4]	95.1%	91.4%	512	9K
Full Capacity Unitary RNN [5]	96.9%	94.1%	512	270K
Soft orthogonal RNN [7]	94.1%	91.4%	128	18K
Cayley RNN [53]	98.2%	96.5%	512	137K
Kronecker RNN [29]	96.4%	94.5%	512	11K
Fast GRNN [54]	98.7%	-	-	-
Antisymmetric RNN [21]	98.0%	95.8%	128	10K
Incremental RNN [55]	98.1%	95.6%	-	-
Non-normal RNN [8]	-	96.5%	512	269K
Exponential RNN [9]	98.7%	96.6%	512	137K
Lipschitz RNN (ours)	98.1%	92.3%	64	9K
Lipschitz RNN (ours)	99.0%	97.2%	128	34K

TABLE 2. Evaluation accuracy on pixel-by-pixel CIFAR10 and noise padded CIFAR10.

Name	ordered	noise padded	N	# parms
LSTM baseline by [21]	59.7%	11.6%	128	69K
Antisymmetric RNN [21]	58.7%	48.3%	256	36K
Incremental RNN [55]	-	54.5%	-	-
Lipschitz RNN (ours)	63.2%	55.2%	256	134K

A variation of this problem is the noise-padded CIFAR10 problem [21], where we consider each row of an image as input at time step t . (Here, we stack the rows from each channel so that we obtain an input of dimension $x \in \mathbb{R}^{96}$.) Then, after 32 time steps, we start to feed the recurrent unit with independent standard Gaussian noise for 968 time steps. At the final point in $T = 1000$, we use the learned hidden state for classification. This problem is challenging because only the first 32 time steps contain signals. Thus, the recurrent unit needs to recall information from along time ago.

Table 2 provides a summary of our results. Our Lipschitz recurrent unit outperforms both the incremental RNN [55] and the antisymmetric RNN [21] by a significant margin. This impressively demonstrates that the Lipschitz unit enables the stable propagation of signals over long time horizons.

6.3 Ablation Study

The performance of the Lipschitz recurrent unit is due to two main innovations: (i) the additional linear term; and (ii) the scheme for constructing the hidden-to-hidden matrices A and W in Eq. (9). Thus, we investigate the effect of both innovations, while keeping all other conditions fixed.

More concretely, we consider the following ablation recurrent unit

$$(16) \quad h_t = h_{t-1} + \alpha \cdot \epsilon \cdot Ah_{t-1} + \epsilon \cdot \tanh(z_t), \quad \text{with} \quad z_t = Wh_{t-1} + Ux_t + b,$$

where α controls the effect of the linear hidden unit. Both A and W depend on the parameters β, γ .

Figure 2a studies the effect of the linear hidden unit, with $\beta = 0.65$ for the ordered task and $\beta = 0.8$ for the permuted task. In both cases we use $\gamma = 0.001$. It can be seen that the test accuracies of both the ordered and permuted pixel-by-pixel MNIST tasks clearly depend on the linear hidden unit.

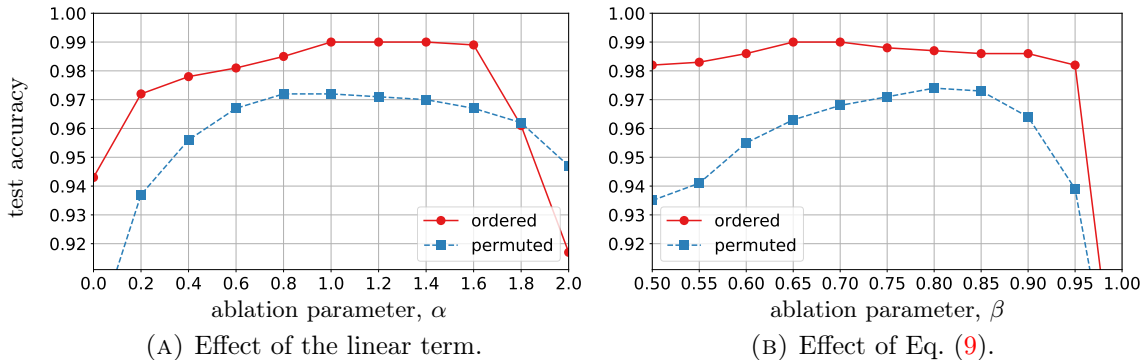


FIGURE 2. The ablation study examines the effect of the linear term Ah (in (a)) and the importance of the Skew-Symmetric Decomposition for constructing the hidden-to-hidden matrices (in (b)).

For $\alpha = 0$, our models reduces to simple neural ODE recurrent units. The recurrent unit degenerates for $\alpha > 1.6$, since the external input is superimposed by the hidden state.

Figure 2b studies the effect of the hidden-to-hidden matrices with respect to β . It can be seen that $\beta = \{0.65, 0.70\}$ achieves peak performance for the ordered task, and $\beta = \{0.8, 0.85\}$ does so for the permuted task. Note that $\beta = 1.0$ recovers an antisymmetric hidden-to-hidden matrix.

6.4 Robustness with Respect to Input and Parameter Perturbations

In the following, we study the robustness (structural stability) of the Lipschitz recurrent unit with respect to input and parameter perturbations. Our results demonstrate that the Lipschitz recurrent unit is a robust unit that is less affected by small (input or parameter) perturbations, as compared to other units.

Input perturbation analysis. Here, we study the sensitivity of the response y_T at time T in terms of the test accuracy with respect to a sequence of perturbed inputs $\{\tilde{x}_1, \dots, \tilde{x}_T\} \in \mathbb{R}^8$. For computational ease, we consider sequences that have length $T = 98$, *i.e.*, we split each MNIST thumbnail into 98 sequences of length 8.

Let $X \in \mathbb{R}^{28 \times 28}$ be a thumbnail. First, we consider additive *white noise perturbations*, $\tilde{X} = X + \Delta X$, where the additive noise term is drawn from the standard normal distribution $\Delta x \sim \mathcal{N}(0, \sigma)$. This perturbation strategy emulates measurement errors that can result from data acquisition with poor sensors. In addition, we consider *salt and pepper perturbations* (also known as impulse noise). This perturbation strategy emulates, for instance, defective pixels that result from converting analog signals to digital signals, and the noise model takes the following form

$$(17) \quad Pr(\tilde{X} = X) = 1 - \alpha,$$

$$(18) \quad Pr(\tilde{X} = \max) = \alpha/2,$$

$$(19) \quad Pr(\tilde{X} = \min) = \alpha/2,$$

where $\tilde{X}(i, j)$ denotes the corrupted image, α controls the amount of defective pixels and *min* and *max* denote to the minimum and maximum pixel values.

Figure 3 shows the results for our Lipschitz RNN for these two noise models, compared with three different continuous-time recurrent units, all of which were trained with an explicit Euler scheme. It can be seen that the Lipschitz unit is less sensitive to input perturbations, as compared to a simple neural ODE RNN, an antisymmetric RNN, and unitary RNN.

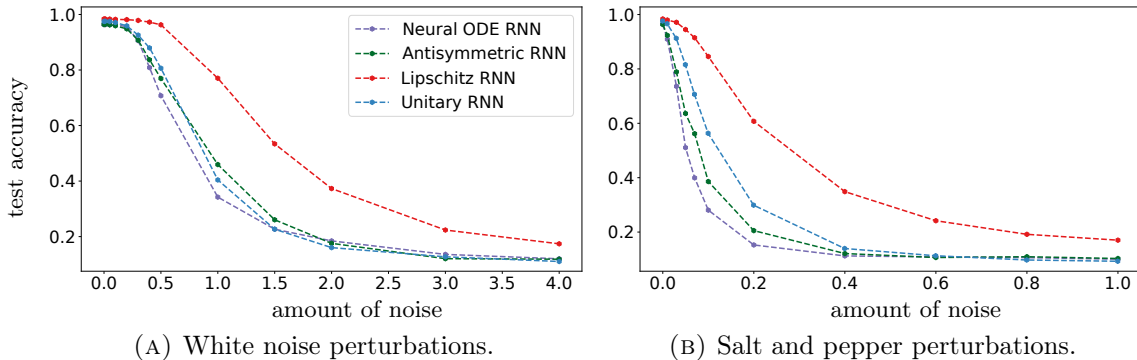


FIGURE 3. Sensitivity with respect to different input perturbations.

Next, we consider artificially constructed perturbations (so called adversarial examples) [56]. Such adversarial examples can be constructed by using optimization based strategies that seek a perturbation ΔX which maximizes the loss ℓ of the model F

$$(20) \quad \underset{\|\Delta X\|_p \leq r}{\text{maximize}} \quad \ell(F_\theta(X + \Delta X), y),$$

with the constraint that the norm of the perturbation is less than or equal to r . The choice of different norm ball perturbations and different optimization methods leads to different adversarial examples. Here, we consider the projected gradient decent (PGD) [57] and DeepFool [58] methods, with l_2 and l_∞ norm ball perturbations. We construct the adversarial examples with full access to the models, using 7 iterations. The step size for PGD is set to 0.01. The results are presented in Table 3, showing that the Lipschitz RNN is more resilient, as compared to the two other units.

Hessian analysis. Here, we consider eigenanalysis of the Hessian, which provides a powerful tool for studying various aspects of deep neural networks [59, 60, 61, 62]. Specifically, we study the Hessian spectrum with respect to the model parameters of the recurrent unit. The Hessian matrix H with respects to the weights $\theta = \{A, W, U\}$ of the recurrent unit is a $K \times K$ symmetric matrix of second partial derivatives (*i.e.*, the Jacobian of the Jacobian of the model at hand):

$$(21) \quad H(\theta_t)_{i,j} = \left. \frac{\partial^2 \mathcal{L}}{\partial \theta_i \partial \theta_j} \right|_{\theta = \theta_t},$$

where \mathcal{L} is the loss function that was used for training and $H(\theta)$ is the local loss curvature at θ .

The Hessian provides us with insights about the curvature of the loss function. This is because the Hessian is defined as the derivatives of the gradients, and thus the Hessian eigenvalues describe the change in the gradient of \mathcal{L} as we take an infinitesimal step into a given direction.

TABLE 3. Summary of various input perturbation strategies and results for Hessian-based robustness metrics. The models have been trained to solve the ordered pixel-by-pixel MNIST problem, where the length of input sequence is set to $T = 98$. The Lipschitz recurrent unit performs best across all metrics.

Model	PGD	DF ₂	DF _∞	$\lambda_{max}(H)$	$tr(H)$	$\kappa(H)$
Neural ODE RNN	88.5%	69.6%	44.5%	0.30	4.7	37.6
Antisymmetric RNN	84.7%	83.4%	44.3%	0.24	4.8	35.5
Lipschitz RNN (ours)	93.0%	89.2%	54.1%	0.14	3.1	23.2

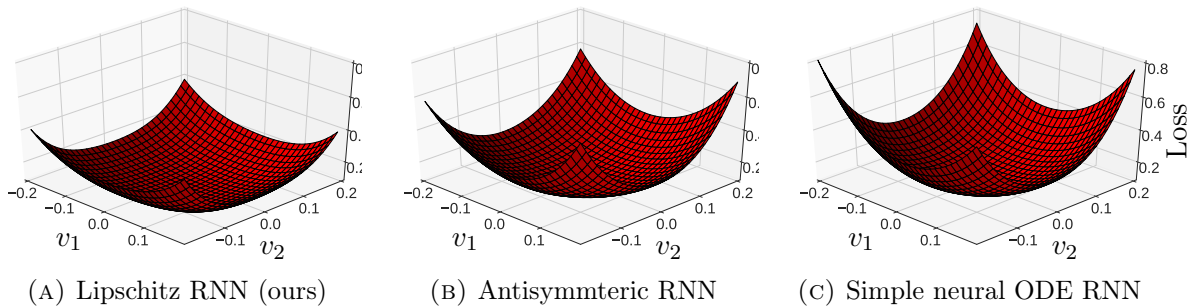


FIGURE 4. Loss landscapes along the two dominant components of the Hessian for the Lipschitz RNN (a), the Antisymmetric RNN (b), and a simple neural ODE RNN(c). All three models have roughly the same initial training loss, but the curvature of the loss landscape for the Lipschitz RNN is more smooth. As a result, the Lipschitz RNN is more robust to parameter perturbations.

Given the Hessian, we can formulate an eigenvalue problem $Hv = \lambda v$, where λ represents an eigenvalue and v an eigenvector of the Hessian. The eigenvectors span the (local) surface of the loss function at a given point, and the corresponding eigenvalue determines the curvature in the direction of the eigenvectors. This means that larger eigenvalues indicate a larger curvature, *i.e.*, greater sensitivity, and the sign of the eigenvalues determines whether the curvature will be positive or negative.

Table 3 reports the largest eigenvalue $\lambda_{max}(H)$ and the trace of the Hessian $tr(H)$ (which can be computed efficiently with `PyHessian` [63]). The largest eigenvalue being smaller indicates that our Lipschitz RNN found a flatter minimum, as compared to the simple neural ODE and Antisymmetric RNN. It is known that such flat minima can be perturbed without significantly changing the loss value [59]. To illustrate this, Figure 4 shows the local loss landscapes around the point θ . More concretely, the loss landscape is computed as

$$(22) \quad \tilde{\mathcal{L}} = \frac{1}{K} \sum_{i=1}^K l(F(x_i), y_i; \theta + \eta_1 v_1 + \eta_2 v_2),$$

where η controls the level of the perturbation of θ along the two dominant eigenvectors v_1 and v_2 .

Table 3 also reports the condition number $\kappa(H) := \frac{\lambda_{max}}{\lambda_{min}}$ of the Hessian. The condition number $\kappa(H)$ provides a measure for the spread of the eigenvalues of the Hessian. It is known that first-order methods can slow down in situations where κ is large [64]. From a dynamical systems point of view, κ provides a measure for the stiffness of the corresponding differential equation. The condition number and trace of our Lipschitz RNN being smaller also indicates improved robustness properties.

7 CONCLUSION

In this work, we have viewed RNNs as dynamical systems with input, and we have proposed a novel Lipschitz recurrent unit that excels on a range of benchmark tasks. The special structure of the recurrent unit allows us to study its behavior via *Lyapunov's direct method*. In turn, the insights from this analysis motivated the symmetric-skew decomposition scheme for constructing hidden-to-hidden matrices, which mitigates the *vanishing and exploding gradients problem*. Due to the nice stability properties of the Lipschitz recurrent unit, we also obtain a model that is *more robust with respect to input and parameter perturbations*. This behavior is also reflected by the Hessian analysis of the model. We expect that the improved robustness will make the Lipschitz RNN more reliable for sensitive applications. Research code is shared via github.com/erichson/LipschitzRNN.

ACKNOWLEDGMENTS

We are grateful to the generous support from Amazon AWS and Google Cloud. NBE would like to acknowledge CLTC for providing support of this work. MWM would like to acknowledge ARO, DARPA, NSF, and ONR for providing partial support of this work.

A PROOFS

A.1 Proof for Proposition 1

Lyapunov's stability theorem provides a powerful framework to determine whether a dynamical system is stable. Here, we state it for completeness. For details and a proof of Lyapunov's stability theorem, see [44, 45, 46].

Theorem A.1. *Let h^* be an equilibrium point for $\dot{h} = f(h)$ and $\mathcal{D} \subset \mathbb{R}^N$ be a neighborhood around the equilibrium point h^* . The equilibrium point h^* is*

- *stable if there exists a continuously differentiable function $\mathcal{V} : \mathcal{D} \rightarrow \mathbb{R}$ such that*

$$(23) \quad \mathcal{V}(h^*) = 0,$$

$$(24) \quad \mathcal{V}(h) > 0, \quad \forall h \in \mathcal{D} \setminus h^*,$$

$$(25) \quad \dot{\mathcal{V}}(h) \leq 0, \quad \forall h \in \mathcal{D}.$$

- *asymptotically stable if we have that*

$$(26) \quad \dot{\mathcal{V}}(h) < 0, \quad \forall h \in \mathcal{D} \setminus h^*.$$

We use this theorem to prove the following proposition.

Proposition 1. *An equilibrium point h^* of the differential equation*

$$(27) \quad \dot{h} = Ah + \tanh(Wh + Ux + b),$$

is asymptotically stable if the eigenvalues of the hidden-to-hidden matrix A have negative real parts.

Proof. We use $V(h) = (h - h^*)^\top P(h - h^*)$ as a candidate Lyapunov function, where $P \in \mathbb{R}^{N \times N}$ is a real symmetric positive definite matrix (*i.e.*, $P = P^\top$). We proceed by forming the derivative of the Lyapunov function \mathcal{V} and substituting $\dot{h} = Ah + g(h, x)$ so that we yield

$$(28) \quad \dot{\mathcal{V}}(h) = (h - h^*)^\top P \dot{h} + \dot{h}^\top P(h - h^*)$$

$$(29) \quad = (h - h^*)^\top P(Ah + g(h, x)) + (Ah + g(h, x))^\top P(h - h^*)$$

$$(30) \quad = (h - h^*)^\top (PA + A^\top P)h + 2(h - h^*)^\top P g(h, x)$$

$$(31) \quad \leq -(h - h^*)^\top Q(h - h^*) + 2\|h - h^*\|_2 \|P\|_2 \|g(h, x)\|_2,$$

where Q is symmetric matrix that is defined as (also known as Lyapunov equation)

$$(32) \quad PA + A^\top P = -Q.$$

Note that if all the eigenvalues of A have negative real parts, then for any positive definite matrix Q , there exist a positive definite matrix P that is a unique solution of Eq. (32), see [46] for details.

Next, since $\tanh(Wh + Ux + b)$ is globally Lipschitz and bounded $-1 \leq \tanh(\cdot) \leq 1$, we can find $\delta > 0$ for any $r > 0$ such that

$$(33) \quad \|g(h, x)\| := \|\tanh(Wh + Ux + b) - \tanh(Wh^* + Ux + b)\|_2 \leq \delta \|h - h^*\|_2 \quad \forall \|h\|_2 < r.$$

Further, we can bound $h^\top Q h$ as

$$(34) \quad \lambda_{\min}(Q) \|h - h^*\|_2^2 \leq (h - h^*)^\top Q (h - h^*) \leq \lambda_{\max}(Q) \|h - h^*\|_2^2,$$

so that it follows that

$$(35) \quad \dot{V}(h) \leq -(\lambda_{\min}(Q) - 2\delta \|P\|_2) \|h - h^*\|_2^2.$$

Choosing $\delta < 0.5 \cdot \lambda_{\min}(Q) / \|P\|_2$ ensures that $\dot{V}(h)$ negative definite.

□

Figure 5 illustrates that the level surfaces of the Lyapunov function $V(h) = (h - h^*)^\top P (h - h^*)$ trap the trajectories for different initial conditions $h(0) = h$, if all the eigenvalues of A have negative real parts. (Given A , and choosing $Q = I$, we can solve Eq. (32) for P by using the Bartels-Stewart algorithm [65].)

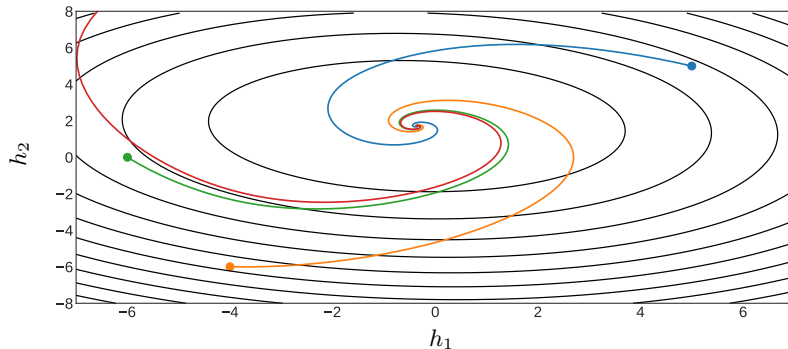


FIGURE 5. Illustration of Lyapunov surfaces in a 2-dimensional space. The black solid lines are level surfaces of $V(h) = h^\top P h$, and the different trajectories correspond to different initial conditions.

A.2 Proof for Proposition 2

First, we show the well-known fact that the eigenvalues of real skew-symmetric matrices, *i.e.*, $A + A^\top = 0$, are zero or purely imaginary. Similar, it can be shown that the eigenvalues of real symmetric matrices, *i.e.*, $A = A^\top$, are zero or real.

Let A be a real $N \times N$ skew-symmetric matrix which satisfies the condition that $A^\top = -A$. Since A is a square matrix, we can formulate the following eigenvalue problem

$$(36) \quad Av = \lambda v,$$

where $v \in \mathbb{C}^N$ is a nonzero eigenvector ($\|v\| \neq 0$) and $\lambda \in \mathbb{C}$ is the corresponding eigenvalue.

We premultiply Eq. (36) on both sides with the conjugate transposed eigenvector \bar{v}^\top

$$(37) \quad \bar{v}^\top Av = \lambda \bar{v}^\top v = \lambda \|v\|^2.$$

Since A is a real and skew-symmetric matrix we have that

$$(38) \quad \bar{v}^\top Av = v^\top A^\top \bar{v} = -v^\top A \bar{v}.$$

Taking complex conjugates of the eigen problem in Eq. 36, we obtain:

$$(39) \quad A\bar{v} = \bar{\lambda}\bar{v} = \bar{\lambda}\bar{v},$$

Then, substituting Eq. (39) into Eq. (38) yields

$$(40) \quad -v^\top A\bar{v} = -\bar{\lambda}v^\top \bar{v} = -\bar{\lambda}\|v\|^2.$$

Finally, we substitute Eq. (40) back into Eq. 37 and yield

$$(41) \quad -\bar{\lambda}\|v\|^2 = \lambda\|v\|^2.$$

It follows that $-\bar{\lambda} = \lambda$, which in turn implies that λ is either zero or a purely imaginary number.

Now, we can prove the following proposition.

Proposition 2. *Let $A_{\beta,\gamma} \in \mathbb{R}^{N \times N}$, with $\beta = [0.5, 1]$ and $\gamma \geq 0$, be constructed via*

$$(42) \quad A_{\beta,\gamma} = (1 - \beta) \cdot (M + M^T) + \beta \cdot (M - M^T) - \gamma I.$$

Then, the real parts of the eigenvalues $\mathcal{R}\lambda_i(A_{\beta,\gamma})$, $i = 1, 2, \dots, N$, are bounded by

$$(43) \quad (1 - \beta) \mathcal{R}\lambda_{\min}(M_{sym}) - \gamma \leq \mathcal{R}\lambda_i(A_{\beta,\gamma}) - \gamma \leq (1 - \beta) \mathcal{R}\lambda_{\max}(M_{sym}) - \gamma,$$

with $M_{sym} := M + M^T$ and $M_{skew} := M - M^T$, where M is an arbitrary real $N \times N$ matrix.

Proof. We know that the eigenvalues of M_{sym} are real and satisfy

$$(44) \quad \langle x, M_{sym}x \rangle \leq \lambda_{\max}(M_{sym})\|x\|^2,$$

$$(45) \quad \langle x, M_{sym}x \rangle \geq \lambda_{\min}(M_{sym})\|x\|^2,$$

where $\langle \cdot, \cdot \rangle$ is the standard inner product and x is an eigenvector with eigenvalue λ . Further, since M_{skew} is a real matrix, the adjoint is equal to the transpose so that

$$(46) \quad \langle M_{skew}x, x \rangle = \langle x, M_{skew}^T x \rangle = \langle x, -M_{skew}x \rangle.$$

Hence, we also know that

$$(47) \quad \langle x, M_{skew}x \rangle \leq \lambda_{\max}(M_{skew})\|x\|^2,$$

$$(48) \quad \langle x, M_{skew}x \rangle \geq \lambda_{\min}(M_{skew})\|x\|^2.$$

Now, starting with $\langle x, A_{\beta,\gamma}x \rangle$, where $\gamma = 0$, we derive the following statement

$$(49) \quad \langle x, ((1 - \beta)M_{sym} + \beta M_{skew})x \rangle = \langle x, (1 - \beta)M_{sym}x \rangle + \langle x, \beta M_{skew}x \rangle$$

$$(50) \quad \leq (1 - \beta)\lambda_{\max}(M_{sym})\|x\|^2 + \beta\lambda_{\max}(M_{skew})\|x\|^2.$$

It follows that the real part of the largest eigenvalue of $A_{\beta,\gamma}$ is bounded by

$$(51) \quad \mathcal{R}\lambda_{\max}(A_{\beta,\gamma}) \leq (1 - \beta)\mathcal{R}\lambda_{\max}(M_{sym}) + \beta\mathcal{R}\lambda_{\max}(M_{skew}).$$

Since, the eigenvalues of M_{skew} are either zero or purely imaginary, we conclude that

$$(52) \quad \mathcal{R}\lambda_{\max}(A_{\beta,\gamma}) \leq (1 - \beta)\mathcal{R}\lambda_{\max}(M_{sym}).$$

By the same argument, we can conclude that

$$(53) \quad \mathcal{R}\lambda_{\min}(A_{\beta,\gamma}) \geq (1 - \beta)\mathcal{R}\lambda_{\min}(M_{sym}).$$

Assuming that the eigenvalues of $A_{\beta,\gamma}$ are weakly ordered $\lambda_1 \geq \lambda_i \geq \dots \lambda_N$, we yield that

$$(54) \quad (1 - \beta)\mathcal{R}\lambda_{\min}(M_{sym}) \leq \mathcal{R}\lambda_i(A_{\beta,\gamma}) \leq (1 - \beta)\mathcal{R}\lambda_{\max}(M_{sym}).$$

Finally, it is easy to show that γ shifts the eigenvalue λ to $\lambda - \gamma$. This follows from the eigenvalue problem. Specifically, we have

$$(55) \quad (A_{\beta,\gamma} - \gamma I)v = (\lambda - \gamma)v.$$

□

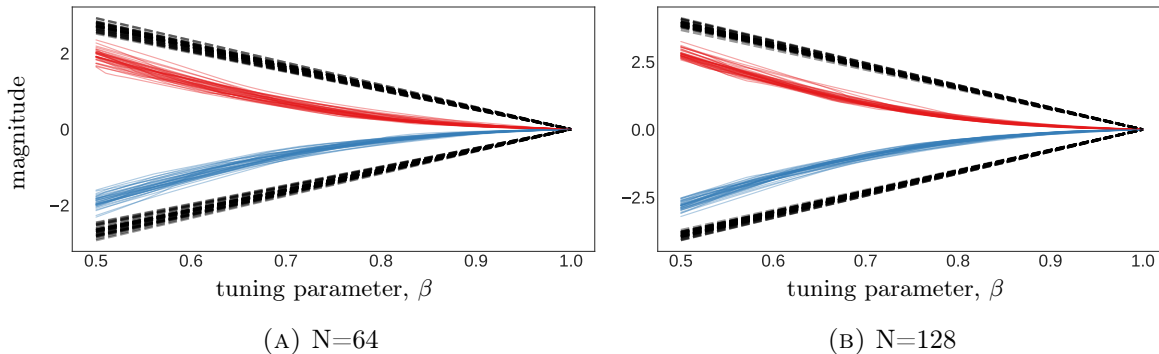


FIGURE 6. Empirical evaluation of the theoretical bound (Eq. (43)). The red lines track the largest real part and the blue lines track the smallest real part of the eigenvalues of the hidden-to-hidden matrix A_β . Each line corresponds to a different hidden-to-hidden matrix of dimension $N = 64$ in (a) and $N = 128$ in (b). The dashed black lines indicate the theoretical bound for each trial.

Note, that it follows that we always can chose $\gamma > \mathcal{R}\lambda_{max}(A_{beta})$ so that the Lyapunov equation

$$(56) \quad P(A_\beta - \gamma I) + (A_\beta - \gamma I)^\top P = -Q$$

has a unique solution.

Figure 6 illustrates the effect of β onto the eigenvalues of $A_{\beta,\gamma}$ with the largest and smallest real parts. It can be seen, both empirically and theoretically, that the real part of the eigenvalues converges towards zero as β tends towards one, *i.e.*, we yield a skew-symmetric matrix with purely imaginary eigenvalues in the limit. Thus, for a sufficiently large parameter β we yield a system that approximately preserves an “energy” for a limited time-horizon

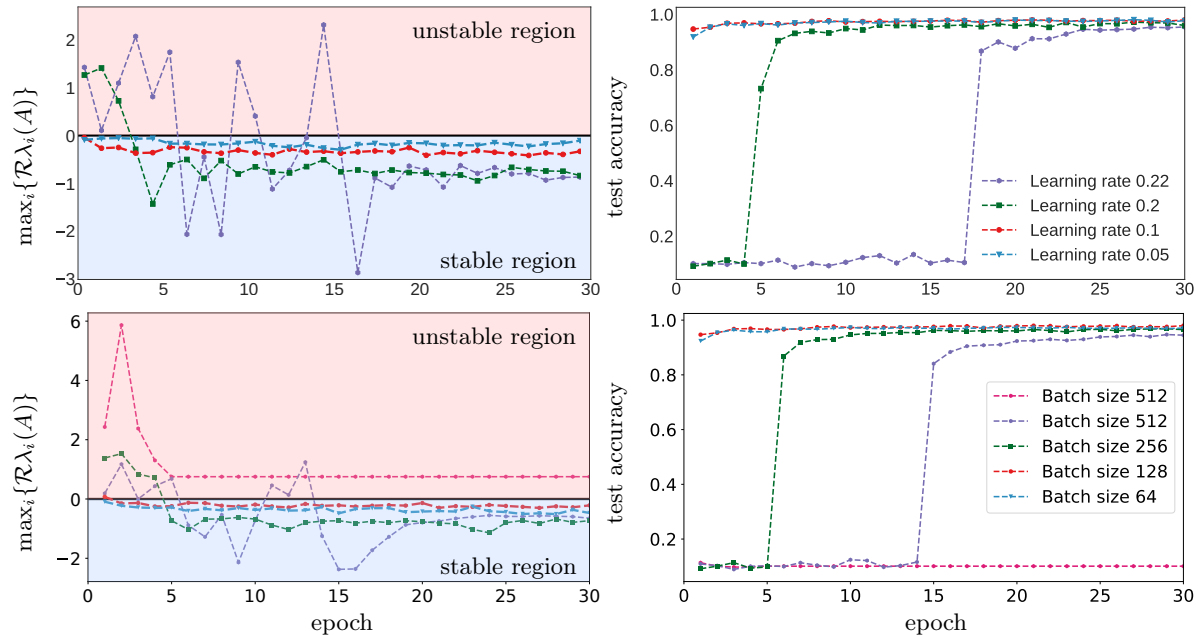
$$(57) \quad \mathcal{R}\lambda_i(A_{\beta,\gamma}) \approx 0, \quad \text{for } i = 1, 2, \dots, N.$$

B A NOTE ON STABILITY AND GENERALIZATION

Here, we study the relationship between stability and generalization performance of the Lipschitz RNN. Recall, that the Lipschitz recurrent unit is stable if all eigenvalues of $A_{\beta,\gamma}$ have negative real parts (*i.e.*, $\mathcal{R}\lambda_i(A) < 0$) and unstable otherwise.

Figure 7a plots the largest real part $\max_i\{\mathcal{R}\lambda_i(A_{\beta,\gamma})\}$, with $\beta = 0.65$ and $\gamma = 0.001$, for models that are trained with different learning rates (first row); a for models that are trained with different batch sizes (second row). Figure 7b shows the corresponding test accuracy.

We see (first row) that models trained with large learning rates show an initially unstable behavior. Further, the results show that such a model that has an eigenvalues $\mathcal{R}\lambda_i(A) > 0$ does not learn anything meaningful. We see (second row) a similar behavior for models that are trained with large batch sizes, *i.e.*, such models tend to be unstable and have low predictive accuracy. On the other hand, models that are trained with small learning rates or small batch sizes learn a hidden-hidden-matrix A that is stable and obtain good predictive performance.



(A) Performance through the lens of stability (B) Performance in terms of generalization error

FIGURE 7. Performance of the Lipschitz RNN through the lens of stability (a) and generalization performance (b). The top rows show results for models trained with different learning rates, and the bottom row shows models trained with different batch sizes. It can be seen that stability provides a data-agnostic tool to investigate the performance of the unit, *i.e.*, the models learn only in the stable region (blue plane), while they do not learn anything meaningful in the unstable region (red plane).

C TUNING PARAMETERS

Recall our model formulation

$$(58) \quad h_{t+1} = h_t + \int_t^{t+\Delta t} Ah(t) + \tanh(Wh(t) + Ux(t)) dt$$

$$(59) \quad \approx \text{ODESolve}[Ah + \tanh(Wh + Ux), h_t, \Delta t]$$

$$(60) \quad = h_t + \Delta t \cdot \text{scheme}[Ah_t + \tanh(Wh_t + Ux_t), h_t, \Delta t].$$

For our experiments, we use the forward Euler scheme that yields the following discretization:

$$(61) \quad h_t = h_{t-1} + \alpha \cdot \epsilon \cdot Ah_{t-1} + \epsilon \cdot \tanh(Wh_{t-1} + z_t), \quad \text{with } z_t = Ux_t + b.$$

Note that we treat the step size ϵ as a tuning parameter, since we do not have prior knowledge about Δt for the experiments that we consider.

Further, we construct hidden-to-hidden weight matrices A and W as

$$(62) \quad A = T(B, \beta, \gamma) := (1 - \beta) \cdot (B + B^T) + \beta \cdot (B - B^T) - \gamma I,$$

$$(63) \quad W = T(C, \beta, \gamma) := (1 - \beta) \cdot (C + C^T) + \beta \cdot (C - C^T) - \gamma I.$$

Note that B and C have the same dimensions as A and W . The parameter γ introduces a small amount of regularization, *i.e.*, it shifts the real part of the eigenvalues of A and B left by γ . We initialize the hidden-to-hidden matrices by sampling weights from the normal distribution $\mathcal{N}(0, \sigma)$, where σ is the variance.

TABLE 4. Tuning parameters used for our experimental results and the performance evaluated with 12 different seed values for the parameter initialization of the model.

Name	N	learning rate	decay	β	γ	ϵ	σ	Max	Min	Avg.
Ordered MNIST	64	0.1	0.2	0.65	0.001	0.01	16/64	0.981	0.976	0.979
Ordered MNIST	128	0.1	0.2	0.65	0.001	0.01	32/128	0.990	0.984	0.987
Permuted MNIST	64	0.1	0.2	0.8	0.001	0.01	16/128	0.923	0.915	0.918
Permuted MNIST	128	0.1	0.2	0.8	0.001	0.01	32/128	0.972	0.968	0.970
Ordered CIFAR10	256	0.1	0.2	0.65	0.001	0.01	6/256	0.632	0.606	0.623
Noise-padded CIFAR10	256	0.1	0.2	0.75	0.001	0.01	6/256	0.552	0.537	0.545

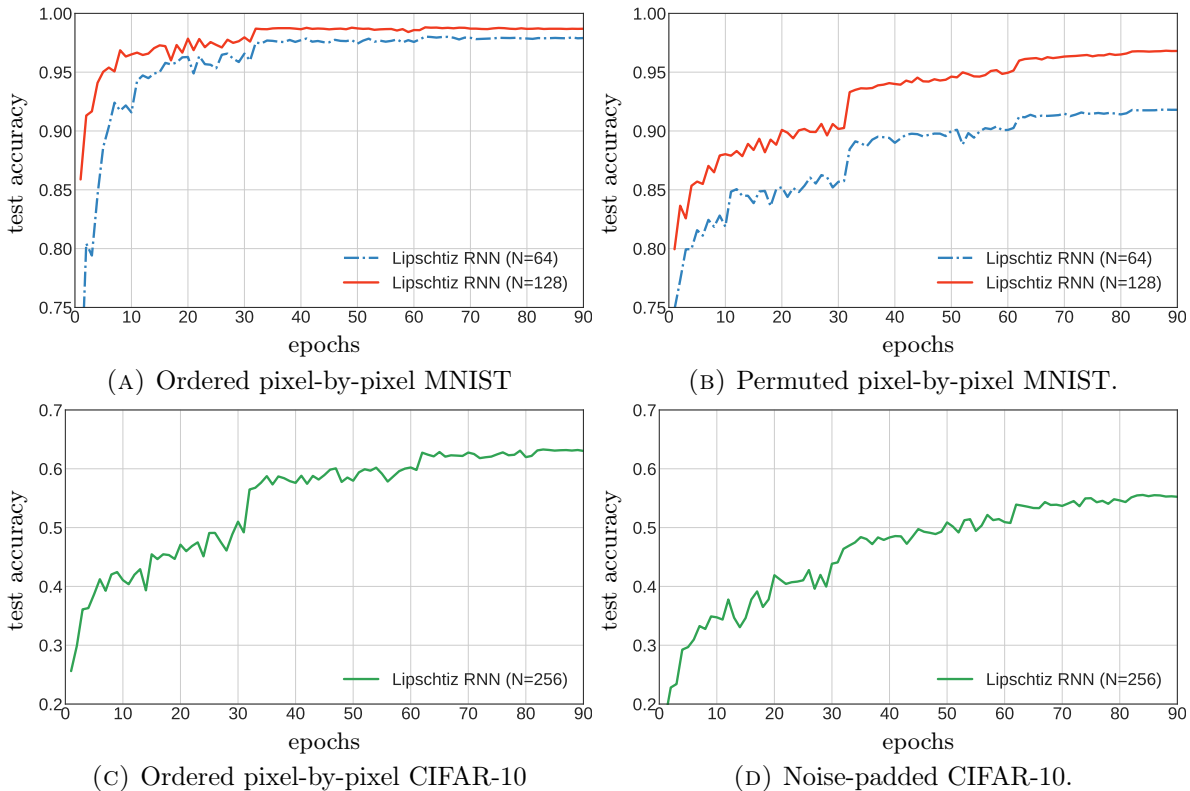


FIGURE 8. Test accuracies for the Lipschitz RNN for different classification tasks.

We use stochastic gradient descent (SGD) with momentum 0.9 for learning the weights. We train all our models for 90 epochs, with scheduled learning rate decays at epochs $\{30, 60, 80\}$. The tuning parameters are summarized in Table 4. In addition, we list the minimum (min), maximum (max) and average (avg.) test accuracies for the models evaluated with 12 different seed values. Figure 8 shows the test accuracy curves for our Lipschitz RNN for the different classification tasks.

REFERENCES

- [1] G. E. Hinton, "Learning distributed representations of concepts," in *Conference of the Cognitive Science Society*, vol. 1, 1986, p. 12.
- [2] Y. Bengio, P. Simard, and P. Frasconi, "Learning long-term dependencies with gradient descent is difficult," *IEEE Transactions on Neural Networks*, vol. 5, no. 2, pp. 157–166, 1994.
- [3] R. Pascanu, T. Mikolov, and Y. Bengio, "On the difficulty of training recurrent neural networks," in *International Conference on Machine Learning*, 2013, pp. 1310–1318.
- [4] M. Arjovsky, A. Shah, and Y. Bengio, "Unitary evolution recurrent neural networks," in *International Conference on Machine Learning*, 2016, pp. 1120–1128.
- [5] S. Wisdom, T. Powers, J. Hershey, J. Le Roux, and L. Atlas, "Full-capacity unitary recurrent neural networks," in *Advances in Neural Information Processing Systems*, 2016, pp. 4880–4888.
- [6] Z. Mhammedi, A. Hellicar, A. Rahman, and J. Bailey, "Efficient orthogonal parametrisation of recurrent neural networks using householder reflections," in *International Conference on Machine Learning*, 2017, pp. 2401–2409.
- [7] E. Vorontsov, C. Trabelsi, S. Kadoury, and C. Pal, "On orthogonality and learning recurrent networks with long term dependencies," in *International Conference on Machine Learning*, 2017, pp. 3570–3578.
- [8] G. Kerg, K. Goyette, M. P. Touzel, G. Gidel, E. Vorontsov, Y. Bengio, and G. Lajoie, "Non-normal recurrent neural network (nnRNN): Learning long time dependencies while improving expressivity with transient dynamics," in *Advances in Neural Information Processing Systems*, 2019, pp. 13 591–13 601.
- [9] M. Lezcano-Casado and D. Martinez-Rubio, "Cheap orthogonal constraints in neural networks: A simple parametrization of the orthogonal and unitary group," in *International Conference on Machine Learning*, 2019, pp. 3794–3803.
- [10] F. E. Thau, "Observing the state of non-linear dynamic systems," *International Journal of Control*, vol. 17, no. 3, pp. 471–479, 1973.
- [11] D. Dawson, Z. Qu, and J. Carroll, "On the state observation and output feedback problems for nonlinear uncertain dynamic systems," *Systems & Control Letters*, vol. 18, no. 3, pp. 217–222, 1992.
- [12] R. Rajamani, "Observers for Lipschitz nonlinear systems," *IEEE Transactions on Automatic Control*, vol. 43, no. 3, pp. 397–401, 1998.
- [13] K.-i. Funahashi and Y. Nakamura, "Approximation of dynamical systems by continuous time recurrent neural networks," *Neural networks*, vol. 6, no. 6, pp. 801–806, 1993.
- [14] Y. H. Kim, F. L. Lewis, and C. T. Abdallah, "Nonlinear observer design using dynamic recurrent neural networks," in *Proceedings of 35th IEEE Conference on Decision and Control*, vol. 1. IEEE, 1996, pp. 949–954.
- [15] T. W. Chow and X.-D. Li, "Modeling of continuous time dynamical systems with input by recurrent neural networks," *IEEE Transactions on Circuits and Systems I: Fundamental Theory and Applications*, vol. 47, no. 4, pp. 575–578, 2000.
- [16] S. Hu and J. Wang, "Global stability of a class of continuous-time recurrent neural networks," *IEEE Transactions on Circuits and Systems I: Fundamental Theory and Applications*, vol. 49, no. 9, pp. 1334–1347, 2002.
- [17] X.-D. Li, J. K. Ho, and T. W. Chow, "Approximation of dynamical time-variant systems by continuous-time recurrent neural networks," *IEEE Transactions on Circuits and Systems II: Express Briefs*, vol. 52, no. 10, pp. 656–660, 2005.
- [18] A. P. Trischler and G. M. D'Eleuterio, "Synthesis of recurrent neural networks for dynamical system simulation," *Neural Networks*, vol. 80, pp. 67–78, 2016.
- [19] J. Miller and M. Hardt, "Stable recurrent models," in *International Conference on Learning Representations*, 2019.
- [20] S. Hochreiter and J. Schmidhuber, "Long short-term memory," *Neural computation*, vol. 9, no. 8, pp. 1735–1780, 1997.
- [21] B. Chang, M. Chen, E. Haber, and E. Chi, "AntisymmetricRNN: A dynamical system view on recurrent neural networks," in *International Conference on Learning Representations*, 2019.
- [22] W. McCulloch and W. Pitts, "A logical calculus of the ideas immanent in nervous activity," *The bulletin of Mathematical Biophysics*, vol. 5, no. 4, pp. 115–133, 1943.
- [23] E. Caianiello, "Outline of a theory of thought-processes and thinking machines," *Journal of Theoretical Biology*, vol. 1, no. 2, pp. 204–235, 1961.
- [24] F. Rosenblatt, "Principles of neurodynamics: Perceptrons and the theory of," *Brain Mechanisms*, pp. 555–559, 1962.
- [25] D. E. Rumelhart, G. E. Hinton, and R. J. Williams, "Learning representations by back-propagating errors," *Nature*, vol. 323, no. 6088, pp. 533–536, 1986.
- [26] M. I. Jordan, "Serial order: A parallel distributed processing approach," in *Advances in Psychology*. Elsevier, 1997, vol. 121, pp. 471–495.
- [27] J. Elman, "Finding structure in time," *Cognitive Science*, vol. 14, no. 2, pp. 179–211, 1990.

- [28] L. Jing, Y. Shen, T. Dubcek, J. Peurifoy, S. Skirlo, Y. LeCun, M. Tegmark, and M. Soljačić, “Tunable efficient unitary neural networks (EUNN) and their application to RNNs,” in *International Conference on Machine Learning*, 2017, pp. 1733–1741.
- [29] C. Jose, M. Cisse, and F. Fleuret, “Kronecker recurrent units,” in *International Conference on Machine Learning*, 2018, pp. 2380–2389.
- [30] M. Lezcano-Casado, “Trivializations for gradient-based optimization on manifolds,” in *Advances in Neural Information Processing Systems*, 2019, pp. 9154–9164.
- [31] F. J. Pineda, “Dynamics and architecture for neural computation,” *Journal of Complexity*, vol. 4, no. 3, pp. 216–245, 1988.
- [32] B. A. Pearlmutter, “Gradient calculations for dynamic recurrent neural networks: A survey,” *IEEE Transactions on Neural Networks*, vol. 6, no. 5, pp. 1212–1228, 1995.
- [33] Y. Rubanova, T. Chen, and D. Duvenaud, “Latent ordinary differential equations for irregularly-sampled time series,” in *Advances in Neural Information Processing Systems*, 2019, pp. 5321–5331.
- [34] E. De Brouwer, J. Simm, A. Arany, and Y. Moreau, “GRU-ODE-Bayes: Continuous modeling of sporadically-observed time series,” in *Advances in Neural Information Processing Systems*, 2019, pp. 7379–7390.
- [35] M. Y. Niu, L. Horesh, and I. Chuang, “Recurrent neural networks in the eye of differential equations,” *arXiv preprint arXiv:1904.12933*, 2019.
- [36] S. Greydanus, M. Dzamba, and J. Yosinski, “Hamiltonian neural networks,” in *Advances in Neural Information Processing Systems*, 2019, pp. 15 379–15 389.
- [37] Z. Chen, J. Zhang, M. Arjovsky, and L. Bottou, “Symplectic recurrent neural networks,” in *International Conference on Learning Representations*, 2019.
- [38] A. Sanchez-Gonzalez, V. Bapst, K. Cranmer, and P. Battaglia, “Hamiltonian graph networks with ODE integrators,” *arXiv preprint arXiv:1909.12790*, 2019.
- [39] Y. Fu, S. Saab, A. Ray, and M. Hauser, “A dynamically controlled recurrent neural network for modeling dynamical systems,” *arXiv preprint arXiv:1911.00089*, 2019.
- [40] S. Pawar, S. E. Ahmed, O. San, A. Rasheed, and I. M. Navon, “Long short-term memory embedded nudging schemes for nonlinear data assimilation of geophysical flows,” *arXiv preprint arXiv:2005.11296*, 2020.
- [41] M. Cranmer, S. Greydanus, S. Hoyer, P. Battaglia, D. Spergel, and S. Ho, “Lagrangian neural networks,” *arXiv preprint arXiv:2003.04630*, 2020.
- [42] N. B. Erichson, M. Muehlebach, and M. W. Mahoney, “Physics-informed autoencoders for Lyapunov-stable fluid flow prediction,” *arXiv preprint arXiv:1905.10866*, 2019.
- [43] O. Azencot, N. B. Erichson, V. Lin, and M. W. Mahoney, “Forecasting sequential data using consistent Koopman autoencoders,” *arXiv preprint arXiv:2003.02236*, 2020.
- [44] W. Hahn, *Stability of motion*. Springer, 1967, vol. 138.
- [45] S. Sastry, *Nonlinear systems: Analysis, stability, and control*. Springer Science, 2013, vol. 10.
- [46] H. Khalil, *Nonlinear Systems*, ser. Pearson Education. Prentice Hall, 2002.
- [47] T. Chen, Y. Rubanova, J. Bettencourt, and D. Duvenaud, “Neural ordinary differential equations,” in *Advances in neural information processing systems*, 2018, pp. 6571–6583.
- [48] L. Ruthotto and E. Haber, “Deep neural networks motivated by partial differential equations,” *Journal of Mathematical Imaging and Vision*, pp. 1–13, 2019.
- [49] U. Ascher, S. Ruuth, and B. Wetton, “Implicit-explicit methods for time-dependent partial differential equations,” *SIAM Journal on Numerical Analysis*, vol. 32, no. 3, pp. 797–823, 1995.
- [50] E. Haber, K. Lensink, E. Treister, and L. Ruthotto, “IMEXnet a forward stable deep neural network,” in *International Conference on Machine Learning*, 2019, pp. 2525–2534.
- [51] R. J. LeVeque, *Finite Difference Methods for Ordinary and Partial Differential Equations*. Society for Industrial and Applied Mathematics, 2007.
- [52] Q. V. Le, N. Jaitly, and G. E. Hinton, “A simple way to initialize recurrent networks of rectified linear units,” *arXiv preprint arXiv:1504.00941*, 2015.
- [53] K. Helfrich, D. Willmott, and Q. Ye, “Orthogonal recurrent neural networks with scaled cayley transform,” in *International Conference on Machine Learning*, 2018, pp. 1969–1978.
- [54] A. Kusupati, M. Singh, K. Bhatia, A. Kumar, P. Jain, and M. Varma, “Fastgrnn: A fast, accurate, stable and tiny kilobyte sized gated recurrent neural network,” in *Advances in Neural Information Processing Systems*, 2018, pp. 9017–9028.
- [55] A. Kag, Z. Zhang, and V. Saligrama, “RNNs incrementally evolving on an equilibrium manifold: A panacea for vanishing and exploding gradients?” in *International Conference on Learning Representations*, 2020.
- [56] C. Szegedy, W. Zaremba, I. Sutskever, J. B. Estrach, D. Erhan, I. Goodfellow, and R. Fergus, “Intriguing properties of neural networks,” in *International Conference on Learning Representations*, 2014.
- [57] I. J. Goodfellow, J. Shlens, and C. Szegedy, “Explaining and harnessing adversarial examples,” *arXiv preprint arXiv:1412.6572*, 2014.

- [58] S.-M. Moosavi-Dezfooli, A. Fawzi, and P. Frossard, “Deepfool: A simple and accurate method to fool deep neural networks,” in *Conference on Computer Vision and Pattern Recognition*, 2016, pp. 2574–2582.
- [59] S. Hochreiter and J. Schmidhuber, “Flat minima,” *Neural Computation*, vol. 9, no. 1, pp. 1–42, 1997.
- [60] L. Sagun, U. Evci, V. U. Guney, Y. Dauphin, and L. Bottou, “Empirical analysis of the Hessian of over-parametrized neural networks,” *arXiv preprint arXiv:1706.04454*, 2017.
- [61] B. Ghorbani, S. Krishnan, and Y. Xiao, “An investigation into neural net optimization via hessian eigenvalue density,” in *International Conference on Machine Learning*, 2019, pp. 2232–2241.
- [62] Z. Yao, A. Gholami, Q. Lei, K. Keutzer, and M. W. Mahoney, “Hessian-based analysis of large batch training and robustness to adversaries,” in *Advances in Neural Information Processing Systems*, 2018, pp. 4949–4959.
- [63] Z. Yao, A. Gholami, K. Keutzer, and M. W. Mahoney, “PyHessian: Neural networks through the lens of the Hessian,” Tech. Rep., 2019, preprint: arXiv:1912.07145.
- [64] L. Bottou and O. Bousquet, “The tradeoffs of large scale learning,” in *Advances in Neural Information Processing Systems*, 2008, pp. 161–168.
- [65] R. H. Bartels and G. W. Stewart, “Solution of the matrix equation $ax + xb = c$ [f4],” *Communications of the ACM*, vol. 15, no. 9, pp. 820–826, 1972.